Parton distributions and $\cos 2\phi_h$ asymmetry induced by anomalous photon-quark coupling

Xu Cao*

CAS Key Laboratory of High Precision Nuclear Spectroscopy and Center for Nuclear Matter Science, Institute of Modern Physics, Chinese Academy of Sciences, Lanzhou 730000, China and State Key Laboratory of Theoretical Physics, Institute of Theoretical Physics, Chinese Academy of Sciences, Beijing 100190, China

(Received 18 March 2018; published 8 June 2018)

In the spectator models of the nucleon with scalar and axial-vector diquarks, we show the effect of Pauli coupling in the photon-quark vertex to the parton distribution functions (PDFs) of nucleon and azimuthal asymmetry in the unpolarized semi-inclusive deep inelastic scattering (SIDIS). This anomalous coupling gives an obvious contribution to unpolarized and polarized PDFs and also leads to a $\cos 2\phi_h$ azimuthal asymmetry proportional to the squared Pauli form factor, due to the helicity flip of the struck quark. After determining the model parameters by fitting PDFs to the global fits, this new distribution for $\cos 2\phi_h$ asymmetry is given numerically. In the framework of transverse momentum dependence (TMD), we find that it is positive and of a few percent in the kinematical regime of HERMES and COMPASS Collaborations, in the same order of magnitude as the Cahn effect.

DOI: 10.1103/PhysRevD.97.114010

I. INTRODUCTION

The semi-inclusive deep inelastic scattering (SIDIS) not only plays an essential role in studying the parton distribution functions (PDF) of the nucleon, but also its azimuthal asymmetries are important observables related to the transverse spin of quarks inside target hadrons [1]. Two azimuthal moments are present in the unpolarized differential cross sections, with the angular dependence of $\cos\phi_h$ and $\cos 2\phi_h$, respectively (here and afterwards, ϕ_h is the azimuthal angle of produced hadron in the scattering plane). Two main mechanisms for the origin of these asymmetries are usually considered when QCD factorization is applicable. One of them involves the convolution of the Boer-Mulders function [2], which measures the transverse polarization asymmetry of quarks inside an unpolarized hadron and the spin-dependent Collins fragmentation function (FF) of the produced hadron [3,4]. The other one is in terms of the Cahn effect, related to the noncollinear transverse-momentum kinematics. While the former effect is the leading twist one, the latter is kinematically of higher twist. These functions should be either calculated within some phenomenological models [5–8] or be extracted directly from experiments [9–21].

Dirac vector coupling is widely explored in the quark electromagnetic and chromomagnetic current, but the tensor coupling with respect to the anomalous Pauli form factor is less recognized. These Pauli couplings can flip the quark helicity, which is one of the important ingredients to induce single-spin asymmetries (SSA) in SIDIS. It was found that the Pauli couping in quark-gluon vertex from various sources leads to a large SSA in quark-quark scattering [22]. In the hadronic level, possible role of the Pauli-type soft quark-gluon interaction on SSAs in SIDIS was investigated in spectator model [23]. Within the same model, adopting the scalar and axial-vector diquark models for the nucleon, it was recently demonstrated that Pauli couplings in both the quark-photon and quark-gluon vertices produce considerable SSA in SIDIS, whose azimuthal dependencies are the same as that usually called the Collins and Sivers effects [24]. Alternative approaches, e.g., instanton background field [25], MIT bag model [26], and single instanton approximation [27], arrive at similar conclusions. This remarkable mechanism could be promising for our understanding of the large SSAs observed in high-energy hadronic reactions and in SIDIS [1].

The Pauli couplings can be originated from instantons, a small-size strong gluonic fluctuation in the QCD vacuum [28,29]. These nontrivial topological structures of QCD equations generate a very large quark chromomagnatic moment, directly resulting in the Pauli coupling in quark-gluon vertex [30]. It was revealed that this anomalous interaction would play an important role in gluon distributions in the nucleon [31], in quark-gluon plasma [32], in

*caoxu@impcas.ac.cn

high-energy elastic pp scattering [33], and in the $pp \to \pi^0 X$ reaction [34]. In these analyses it was suggested that this quark-gluon interaction would cause the explicit breakdown of transverse-momentum-dependent (TMD) factorization. In addition, the instantons would also give rise to the Pauli coupling in quark–photon vertex, as illustrated within the nonperturbative approach [35,36]. The instanton liquid model [28,29] is widely implemented in the qualitative calculations.

The purpose of this paper is to consider what specifical effects the Pauli coupling of the quark-photon interaction may have on PDFs and unpolarized SIDIS. The contribution of this interaction is expected to be complementary to the Dirac couplings. In Sec. II we give our analytical results of TMD PDFs in spectator models and try to extract the model parameters from the global PDF fits. In Sec. III, we give our new $\cos 2\phi_h$ asymmetry in the framework of TMD factorization and compare it to the Cahn effect. We conclude briefly in Sec. IV.

II. TMD PARTON DISTRIBUTIONS IN SPECTATOR MODELS

In this work, we employ the parton model of nucleon by using the spectator model with scalar and axial-vector diquarks [37], as depicted in Fig 1. We introduce a Pauli coupling besides the conventional Dirac coupling at the vertex between the struck quark and the virtual photon [35]:

$$V_\mu^\gamma = \mathcal{F}_D^q \gamma^\mu - \frac{\mathcal{F}_P^q}{2m_q}\sigma^{\mu\nu}q_\nu \tag{1}$$

with m_q being the constitute quark mass. The $\mathcal{F}_D^q$ and $\mathcal{F}_p^q$ are Dirac and Pauli form factors as a function of photon virtuality $Q^2 = -q^2$, respectively. The perturbative and nonperturbative QCD contributions to the Dirac and Pauli form factor have been calculated with several methods (see [35,38] and references therein). It should be noted that the nonperturbative interaction enters into the model only through above quark-photon vertex. It does not affect the kinematical relationships of involved momenta, but it would influence the virtualities of internal lines of hard scattering. As a matter of fact, it can be easily checked

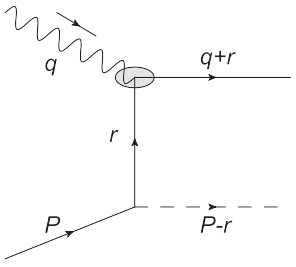

FIG. 1. Diagrammatic representation of the DIS process in our calculation. The blob represents the interaction vertices with both Dirac and Pauli couplings.

that the Pauli coupling $\mathcal{F}_P^q Q/m_q$ present in Eq. (1) is very moderately dependent on Q^2 and roughly follow the order of the usual Diral vector coupling $\mathcal{F}_D^q$ in the instanton liquid model because of the small instanton size (see Eq. (44) hereafter in Sec. III). So it is naively expected this new vertex does not break the TMD factorization between the hard and soft part of SIDIS, and the standard treatment of the convolution between TMD PDFs and FFs can be still used here in the factorization framework [39,40]. Moreover, in our previous calculation of the SSA in SIDIS induced by the Pauli couplings [24], terms which obviously violate order counting in TMD factorization are not present. There we also found that the Pauli coupling in quark-gluon vertex from instanton liquid model does provide appropriate regularization of the loop integrals from final state interaction. In Ref. [26], the Sivers function resulting from this Pauli coupling is successfully calculated by the correlator in terms of gauge links, adopting the same instanton model as ours and the quark wave functions from the MIT bag model. A rigorous proof of the TMD factorization theorem with regard to the Pauli couplings would follow the framework recently proposed within the scalar diquark model in our interested kinematical range and is waiting for future exploration [41].

The nucleon-quark-diquark vertices are chosen to be

$$V_s = ig^s \mathbf{1}, \qquad V_\mu^a = i\frac{g^a}{\sqrt{2}}\gamma_5\gamma^\mu, \tag{2}$$

where the g^s and g^a are couplings in the proton-quark-scalar diquark vertex and proton-quark-axial-vector diquark vertex, respectively. Then the amplitudes of the Born diagram presented in Fig. 1 are straightforwardly written as

$$i\mathcal{A}_{s,s'}^{\lambda} = \frac{-i}{r^2+m_q^2}\bar{u}(q+r,s')\epsilon_\mu^\lambda(q)\left(\mathcal{F}_D^q\gamma^\mu - \frac{\mathcal{F}_P^q}{2m_q}\sigma^{\mu\nu}q_\nu\right) \times (\not{r}+m_q)u(P,s) \tag{3}$$

$$i\mathcal{A}_{s,s'}^{\lambda,\lambda_a} = \frac{-i}{r^2+m_q^2}\bar{u}(q+r,s')\epsilon_\mu^\lambda(q)\left(\mathcal{F}_D^q\gamma^\mu - \frac{\mathcal{F}_P^q}{2m_q}\sigma^{\mu\nu}q_\nu\right) \times (\not{r}+m_q)\frac{\gamma_5}{\sqrt{2}}\not{\epsilon}_D(P-r,\lambda_a)u(P,s) \tag{4}$$

for the scalar and axial-vector diquark models, respectively. Here, the λ and λ_a are helicities of the photon and axial-vector diquark, respectively. The s and s' label the helicities of the initial and final quarks, respectively. The helicity amplitudes are obeying the relations

$$\mathcal{A}_{s,s'}^{\lambda(,\lambda_a)} = -(-1)^{s-s'}\left(\mathcal{A}_{-s,-s'}^{-\lambda(,-\lambda_a)}\right)^*. \tag{5}$$

Following the approach of Hoyer and Jarvinen [23], we work in a coordinate system where the target proton is at rest (laboratory frame) and the virtual photon momentum is

along the $+z$ axis; e.g., the momenta of photon, proton, and struck quark read [23]

$$\begin{aligned} q &= (q^+, q^-, \mathbf{0}_\perp) \simeq (2\nu, -xM, \mathbf{0}_\perp) \\ P &= (P^+, P^-, \mathbf{0}_\perp) \simeq (M, M, \mathbf{0}_\perp) \\ r &= (r^+, r^-, \boldsymbol{r}_\perp) \simeq (xM, xM, r_\perp \cos\phi, r_\perp \sin\phi), \end{aligned} \quad (6)$$

with $\nu = Q^2/2xM$ being the photon energy, M the proton mass, and x the Bjorken variable, respectively. Here, we describe a generic four-vector k as $k = (k^+, k^-, \boldsymbol{k}_\perp)$ and its square $k^2 = (k^+k^- + k^-k^+)/2 + \boldsymbol{k}_\perp^2$. We use $k_\perp$ as the magnitude of $\boldsymbol{k}_\perp$. The polarization vectors of the photon and axial-vector diquark are defined as

$$\epsilon^\lambda(q) = \frac{1}{\sqrt{2}}(0, 0, -\lambda, -i) \quad (7)$$

$$\epsilon_D(P - r, \lambda_a) = \frac{1}{\sqrt{2}}\left(\frac{2(\lambda_a r_x + i r_y)}{(1-x)M}, 0, -\lambda_a, -i\right), \quad (8)$$

where the transversality condition, e.g., $(P - r)\cdot \epsilon_D(P - r, \lambda_a) = 0$, is respected. For simplicity, we define

$$\mathcal{A}^{\lambda(,\lambda_a)}_{s,s'} = g_{s,a}\sqrt{2Mq^+}\frac{1-x}{\boldsymbol{r}_\perp^2 + B_R^2(m_q^2)}\mathcal{I}^{\lambda(,\lambda_a)}_{s,s'}, \quad (9)$$

with $B_R^2(m_q^2) = (1-x)m_q^2 + xm_D^2 - x(1-x)M^2$ and m_D being the diquark mass. After some algebraic calculation, in the limit of $q^+ = Q^2/xM \to \infty$ at fixed k, r, the helicity amplitudes for the scalar diquark model are found to be

$$\mathcal{I}^\lambda_{+,+} \simeq \left(\mathcal{F}_D^q - \frac{\mathcal{F}_P^q}{2m_q}D_Q\right) r_\perp e^{+i\psi}\delta_{\lambda,+1} + \frac{\mathcal{F}_P^q}{2m_q}D_R r_\perp e^{-i\psi}\delta_{\lambda,-1} \quad (10)$$

$$\mathcal{I}^\lambda_{+,-} \simeq -\frac{\mathcal{F}_P^q}{2m_q}\boldsymbol{r}_\perp^2 e^{2i\psi}\delta_{\lambda,+1} + \left(\mathcal{F}_D^q + \frac{\mathcal{F}_P^q}{2m_q}D_R\right)D_R\delta_{\lambda,-1}, \quad (11)$$

with $D_Q = xM - m_q$ and $D_R = xM + m_q$. For the axial-vector diquark model, the full set of amplitudes is

$$\mathcal{I}^{+,+}_{+,+} \simeq -\left(\mathcal{F}_D^q + \frac{\mathcal{F}_P^q}{2m_q}D_R\right)D_R - \frac{\mathcal{F}_P^q}{2m_q}\frac{x}{1-x}\boldsymbol{r}_\perp^2 \quad (12)$$

$$\mathcal{I}^{+,-}_{+,+} \simeq \frac{\mathcal{F}_P^q}{2m_q}\frac{x}{1-x}\boldsymbol{r}_\perp^2 e^{+2i\psi} \quad (13)$$

$$\mathcal{I}^{-,+}_{+,+} \simeq \frac{\mathcal{F}_P^q}{2m_q}\frac{1}{1-x}\boldsymbol{r}_\perp^2 e^{-2i\psi} \quad (14)$$

$$\mathcal{I}^{-,-}_{+,+} \simeq -\frac{\mathcal{F}_P^q}{2m_q}\frac{x}{1-x}\boldsymbol{r}_\perp^2 \quad (15)$$

$$\mathcal{I}^{+,+}_{+,-} \simeq \frac{\mathcal{F}_P^q}{2m_q}D_R r_\perp e^{+i\psi} \quad (16)$$

$$\mathcal{I}^{+,+}_{-,+} \simeq -(\mathcal{F}_D^q + \mathcal{F}_P^q)\frac{x}{1-x}r_\perp e^{-i\psi} \quad (17)$$

$$\mathcal{I}^{+,-}_{-,+} \simeq \left[\mathcal{F}_D^q + \frac{\mathcal{F}_P^q}{2m_q}(xD_R - D_Q)\right]\frac{r_\perp e^{+i\psi}}{1-x} \quad (18)$$

$$\mathcal{I}^{+,-}_{+,-} \simeq 0. \quad (19)$$

The differential cross section of unpolarized and longitudinal polarized DIS is given in terms of the amplitude at tree order in Fig. 1(a),

$$\begin{aligned} \frac{d\sigma}{dx dy d^2\boldsymbol{r}_\perp} &= \frac{1}{Q^4}\sum_{\lambda,\lambda',s,s'}^{(\lambda_a,\lambda'_a)}\Big\{L^{\lambda,\lambda'}\mathcal{A}^{\lambda(,\lambda_a)}_{s,s'}\left(\mathcal{A}^{\lambda'(,\lambda'_a)}_{s,s'}\right)^* \\ &\quad - S_\parallel\sqrt{1-\varepsilon^2}\lambda L^{\lambda,\lambda'}\mathcal{A}^{\lambda(,\lambda_a)}_{s,s'}\left(\mathcal{A}^{\lambda'(,\lambda'_a)}_{s,s'}\right)^*\Big\} \\ &= \frac{16e^2g_{s,a}^2}{xy^2}\frac{y^2}{2(1-\varepsilon)}\left(1 + \frac{\gamma^2}{2x}\right)\left(\frac{1-x}{\boldsymbol{r}_\perp^2 + B_R^2(m_q^2)}\right)^2 \\ &\quad \times \left[\mathcal{N}_+ - \varepsilon\mathcal{N}_- + S_\parallel\sqrt{1-\varepsilon^2}\mathcal{N}_\parallel\right], \end{aligned} \quad (20)$$

with the Bjorken variables y being the fraction of the beam energy carried by the virtual photon. The depolarization factor ε is the ratio of longitudinal and transverse photon flux,

$$\varepsilon = \frac{1 - y - \frac{1}{4}\gamma^2y^2}{1 - y + \frac{1}{2}y^2 + \frac{1}{4}\gamma^2y^2}, \quad (21)$$

with $\gamma = 2xM/Q$. Above we have used the leptonic tensor in the helicity basis:

$$L^{\lambda,\lambda'} = \frac{4e^2Q^2}{y^2}\frac{y^2}{2(1-\varepsilon)}\left(1 + \frac{\gamma^2}{2x}\right)\{\delta_{\lambda,\lambda'} - \varepsilon e^{-2i\lambda\tau}\delta_{\lambda,-\lambda'}\}. \quad (22)$$

Here, τ is the azimuthal angle of the lepton $\boldsymbol{l}_{1\perp} = \boldsymbol{l}_{2\perp} = (l_\perp\cos\tau, l_\perp\sin\tau)$. After some formalism manipulation, we have for the scalar diquark model,

$$\begin{aligned} \mathcal{N}^s_+ &= \sum_\lambda\{|\mathcal{A}^\lambda_{+,+}|^2 + |\mathcal{A}^\lambda_{+,-}|^2\} \\ &\simeq \left(\mathcal{F}_D^q - \frac{\mathcal{F}_P^q}{2m_q}D_Q\right)^2\boldsymbol{r}_\perp^2 + \left(\mathcal{F}_D^q + \frac{\mathcal{F}_P^q}{2m_q}D_R\right)^2D_R^2 \\ &\quad + \left(\frac{\mathcal{F}_P^q}{2m_q}\right)^2\boldsymbol{r}_\perp^2(\boldsymbol{r}_\perp^2 + D_R^2) \\ &\xrightarrow{\mathcal{F}_P^q \sim 0}(\mathcal{F}_D^q)^2(\boldsymbol{r}_\perp^2 + D_R^2) \end{aligned} \quad (23)$$

$$\mathcal{N}^s_- = \mathrm{Re}\sum_\lambda \{\mathcal{A}^\lambda_{+,+}(\mathcal{A}^{-\lambda}_{+,+})^* + \mathcal{A}^\lambda_{+,-}(\mathcal{A}^{-\lambda}_{+,-})^*\} e^{-2i\lambda\tau} \simeq -\left(\frac{\mathcal{F}^q_P}{2m_q}\right)^2 2xMD_R \boldsymbol{r}^2_\perp \cos 2(\psi-\tau) \tag{24}$$

$$\mathcal{N}^s_\parallel = -\sum_\lambda \lambda\{|\mathcal{A}^\lambda_{+,+}|^2 + |\mathcal{A}^\lambda_{+,-}|^2\} \simeq -\left(\mathcal{F}^q_D - \frac{\mathcal{F}^q_P}{2m_q}D_Q\right)^2 \boldsymbol{r}^2_\perp + \left(\mathcal{F}^q_D + \frac{\mathcal{F}^q_P}{2m_q}D_R\right)^2 D^2_R - \left(\frac{\mathcal{F}^q_P}{2m_q}\right)^2 \boldsymbol{r}^2_\perp(\boldsymbol{r}^2_\perp - D^2_R)$$
$$\xrightarrow{\mathcal{F}^q_P\sim 0} (\mathcal{F}^q_D)^2(D^2_R - \boldsymbol{r}^2_\perp). \tag{25}$$

For the axial-vector diquark model, we have

$$\mathcal{N}^a_+ = \sum_{\lambda,\lambda_a}\{|\mathcal{A}^{\lambda,\lambda_a}_{+,+}|^2 + |\mathcal{A}^{\lambda,\lambda_a}_{+,-}|^2\} \simeq \left[\left(\mathcal{F}^q_D + \frac{\mathcal{F}^q_P}{2m_q}D_R\right)D_R + \frac{\mathcal{F}^q_P}{2m_q}\frac{x}{1-x}\boldsymbol{r}^2_\perp\right]^2$$
$$+ \frac{\boldsymbol{r}^2_\perp}{(1-x)^2}\left[(\mathcal{F}^q_D + \mathcal{F}^q_P)^2x^2 + \left(\mathcal{F}^q_D + \frac{\mathcal{F}^q_P}{2m_q}(xD_R - D_Q)\right)^2 + \left(\frac{\mathcal{F}^q_P}{2m_q}\right)^2((1+2x^2)\boldsymbol{r}^2_\perp + (1-x)^2D^2_R)\right]$$
$$\xrightarrow{\mathcal{F}^q_P\sim 0} (\mathcal{F}^q_D)^2\left(D^2_R + \frac{1+x^2}{(1-x)^2}\boldsymbol{r}^2_\perp\right) \tag{26}$$

$$\mathcal{N}^a_- = \mathrm{Re}\sum_{\lambda,\lambda_a}\left\{\mathcal{A}^{\lambda,\lambda_a}_{+,+}(\mathcal{A}^{-\lambda,-\lambda_a}_{+,+})^* + \mathcal{A}^{\lambda,\lambda_a}_{+,-}(\mathcal{A}^{-\lambda,-\lambda_a}_{+,-})^*\right\} e^{-2i\lambda\tau} \simeq -\left(\frac{\mathcal{F}^q_P}{2m_q}\right)^2 \frac{\boldsymbol{r}^2_\perp}{1-x}\left[(1-x)D^2_R + D_RD_Q + \frac{\boldsymbol{r}^2_\perp}{1-x}x(1+x)\right]\cos 2(\psi-\tau) \tag{27}$$

$$\mathcal{N}^a_\parallel = -\sum_{\lambda,\lambda_a}\lambda\{|\mathcal{A}^{\lambda,\lambda_a}_{+,+}|^2 + |\mathcal{A}^{\lambda,\lambda_a}_{+,-}|^2\} \simeq -\left[\left(\mathcal{F}^q_D + \frac{\mathcal{F}^q_P}{2m_q}D_R\right)D_R + \frac{\mathcal{F}^q_P}{2m_q}\frac{x}{1-x}\boldsymbol{r}^2_\perp\right]^2$$
$$+ \frac{\boldsymbol{r}^2_\perp}{(1-x)^2}\left[(\mathcal{F}^q_D + \mathcal{F}^q_P)^2x^2 + \left(\mathcal{F}^q_D + \frac{\mathcal{F}^q_P}{2m_q}(xD_R - D_Q)\right)^2 + \left(\frac{\mathcal{F}^q_P}{2m_q}\right)^2(\boldsymbol{r}^2_\perp - (1-x)^2D^2_R)\right]$$
$$\xrightarrow{\mathcal{F}^q_P\sim 0} (\mathcal{F}^q_D)^2\left(\frac{1+x^2}{(1-x)^2}\boldsymbol{r}^2_\perp - D^2_R\right). \tag{28}$$

As expected, the distributions $\mathcal{N}^{s,a}_+$ and $\mathcal{N}^{s,a}_\parallel$ return back to the results of the conventional diquark models [6] when $\mathcal{F}^q_P$ is approaching zero. Besides, an asymmetric term $\mathcal{N}^{s,a}_-$ with definite angular distribution is generated by the photon-quark Pauli couplings. If we use the Trento convention [42], which uses the angle ϕ_h between the hadron h and lepton planes,

$$\phi_h = \psi - \tau, \tag{29}$$

then the angular dependence of $\mathcal{N}^{s,a}_-$ is $\cos 2(\psi-\tau) = \cos 2\phi_h$, which is identical to those of the Cahn and Boer-Mulders effect. Its physical origin is, however, quite different from the original $\cos 2\phi_h$ azimuthal asymmetries in SIDIS. As can be seen in Eqs. (24) and (27), the magnitudes of $\mathcal{N}^{s,a}_-$ are proportional to the squared Pauli form factor $(\mathcal{F}^q_P)^2$, which is from the nonperturbative contribution and could be explicitly calculated by various phenomenological models, e.g., the instanton liquid model for the nontrivial topological structure of the QCD vacuum [35]. It should be noted that the Pauli couplings $\mathcal{F}^q_P$ introduced in Eq. (44) are Q^2 dependent, which will be discussed in detail in Sec. III.

In our above calculation, we neglect the form factors which are introduced to smoothly suppress the contribution of high transverse momentum. Here, we introduce conventional dipolar form factors in the photon-quark couplings:

$$\mathcal{F}^q_{D,P} \Rightarrow \mathcal{F}^q_{D,P}\frac{r^2 - m_q^2}{(r^2 - \Lambda^2_{s,a})^2} = \mathcal{F}^q_{D,P}\frac{\boldsymbol{r}^2_\perp + B^2_R(m_q^2)}{(\boldsymbol{r}^2_\perp + B^2_R(\Lambda_{s,a}))^2}(x-1). \tag{30}$$

We can read the unpolarized and helicity parton distribution functions (PDFs) from Eqs. (23), (25), (26), and (28),

$$f^s_1(x,\boldsymbol{r}_\perp) = \frac{g^2_s(1-x)^3}{(2\pi)^3}\frac{\mathcal{N}^s_+}{2(\boldsymbol{r}^2_\perp + B^2_R(\Lambda^2_s))^4} \tag{31}$$

$$f^a_1(x,\boldsymbol{r}_\perp) = \frac{g^2_a(1-x)^3}{(2\pi)^3}\frac{\mathcal{N}^a_+}{2(\boldsymbol{r}^2_\perp + B^2_R(\Lambda^2_a))^4} \tag{32}$$

$$g_{1L}^{s}(x,\boldsymbol{r}_\perp)=\frac{g_s^2(1-x)^3}{(2\pi)^3}\frac{\mathcal{N}_\parallel^s}{2(\boldsymbol{r}_\perp^2+B_R^2(\Lambda_s^2))^4} \quad (33)$$

$$g_{1L}^{a}(x,\boldsymbol{r}_\perp)=\frac{g_a^2(1-x)^3}{(2\pi)^3}\frac{\mathcal{N}_\parallel^a}{2(\boldsymbol{r}_\perp^2+B_R^2(\Lambda_a^2))^4}, \quad (34)$$

which return back to the results of the conventional diquark model [23] when $\mathcal{F}_P^q \to 0$. We can also define a new distribution function like the Cahn effect, using Eqs. (24) and (27), as

$$\mathcal{C}^{s}(x,\boldsymbol{r}_\perp)=-\frac{g_s^2(1-x)^3}{(2\pi)^3}\frac{\mathcal{N}_-^s}{2(\boldsymbol{r}_\perp^2+B_R^2(\Lambda_s^2))^4} \quad (35)$$

$$\mathcal{C}^{a}(x,\boldsymbol{r}_\perp)=-\frac{g_a^2(1-x)^3}{(2\pi)^3}\frac{\mathcal{N}_-^a}{2(\boldsymbol{r}_\perp^2+B_R^2(\Lambda_a^2))^4}. \quad (36)$$

In the above equations, $g_{s,a}$ are the normalization factors determined by

$$\int_0^1 \mathrm{d}x \int_0^\infty \mathrm{d}^2\boldsymbol{r}_\perp f_1^{s,a}(x,\boldsymbol{r}_\perp)=\int_0^1 \mathrm{d}x f_1^{s,a}(x)=1. \quad (37)$$

The $\boldsymbol{r}_\perp$-integrated results $f_1^{s,a}(x)$, $g_{1L}^{s,a}(x)$ and $\mathcal{C}^{s,a}(x)$ are given in the Appendix.

After determining the parameters of the model by fitting the known unpolarized and polarized distribution functions $f_1^{u,d}(x)$ and $g_1^{u,d}(x)$, we can predict the numerical results of our model for the $\cos 2\phi_h$ asymmetry. To perform the fit, we need to relate the functions $f_1^{s,a}(x)$ and $g_1^{s,a}(x)$, in terms of diquark types in the model, to the functions $f_1^{u,d}(x)$ and $g_1^{u,d}(x)$ with regard to quark flavors in the global fits. We write them generally as [6,7]

$$f_1^u=c_s^2 f_1^s+c_{a(u)}^2 f_1^{a(u)} \quad (38)$$

$$f_1^d=c_{a(d)}^2 f_1^{a(d)}, \quad (39)$$

which should be generalized to the case of $g_1^{u,d}$ and $\mathcal{C}^{u,d}$. Here, we discriminate the two isospin states of the vector diquark, namely $a(u)$ for the $ud(I_3=0)$ diquark and $a(d)$ for the $uu(I_3=1)$ diquark. We have $c_s^2=3/2$, $c_{a(u)}^2=1/2$ and $c_{a(d)}^2=1$ under the SU(4) symmetry. However, since SU(4) symmetry is no longer strictly preserved in the spectator model of the nucleon, we treat these coefficients instead as free parameters. We have checked that the results are not sensitive to the values of the masses of constituent quark m_q and ud diquark $m_D^{a(u)}$, so we fix them to be

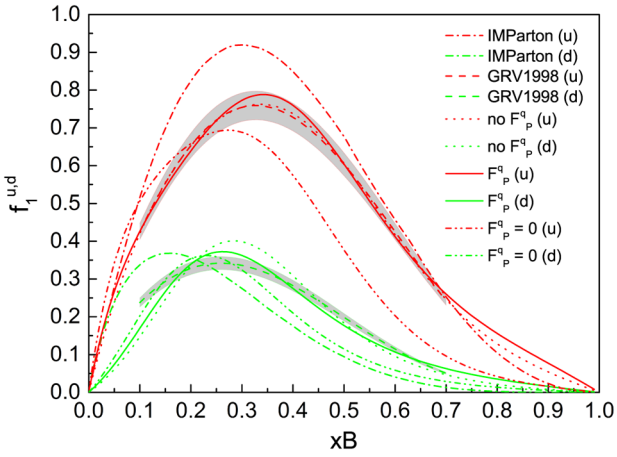

FIG. 2. The unpolarized PDF $f_1^{u,d}$ in our model. The red and blue lines are for u– and d–quark, respectively. The dashed and dash-dotted lines are from GRV1998 [47] and IMParton [50,51], respectively. The shadow bands correspond to the relative error of 5.0% to GRV1998. The dotted and solid curve are the results of Fit-I and Fit-II, respectively. The dash-dot-dotted curves represent result of Fit-II with setting the Pauli coupling in photon-guark vertex to be zero ($\mathcal{F}_P^q=0$).

$m_q=0.30$ GeV and $m_D^{a(u)}=1.5$ GeV. We have, in total, nine free parameters for the model.

In order to reproduce the parametrizations of PDFs extracted from experimental data, we have to choose a proper scale Q_0^2 at which the diquark models are probably appropriate. Following the arguments in Refs. [6,7], a very low scale Q_0^2 seems to be favored, so the lowest possible value of the scale is used in the literature, e.g., 0.3 GeV^2 [6] and 0.078 GeV^2 [7]. Only a few PDFs of the global fit are at hand in such a low Q^2 range, and most of them are usually applicable above 1.0 GeV^2, e.g., CT14 [43], MMHT2014 [44], NNPDF [45], and ABM11 [46]. We fit our model parameters to the leading-order GRV1998 [47] and GRSV2000 [48] parametrization at $Q_0^2=0.26$ GeV^2 for $f_1^{u,d}$ and $g_1^{u,d}$, respectively. We assign a constant relative error of 5.0% to $f_1^{u,d}$ based on comparisons with HERAPDF [49] and IMParton [50,51] under the same Q^2. We allocate a relative error of 20.0% to $g_1^{u,d}$ in view of DNS2005 [52] and DSSV2010 [53] (see Refs. [54,55] for a detailed comparison of various $g_1^{u,d}$).

The fit results are shown in Figs. 2 and 3 for $f_1^{u,d}$ and $g_1^{u,d}$, respectively. The extracted parameters are shown in Table I. In Fit-I, we use the conventional model, in which there is no Pauli coupling in the photon-guark vertex, e.g., setting $\mathcal{F}_P^q=0$ in the fit. We achieve a good agreement except for the g_1^d. The fitted g_1^d goes to positive values in the range of around $x=0.6$, while it is negative in the full x range in GRSV2000. This conclusion has been found before in Ref. [6]. In Fit-II, we use the full model with $\mathcal{F}_P^q$ at

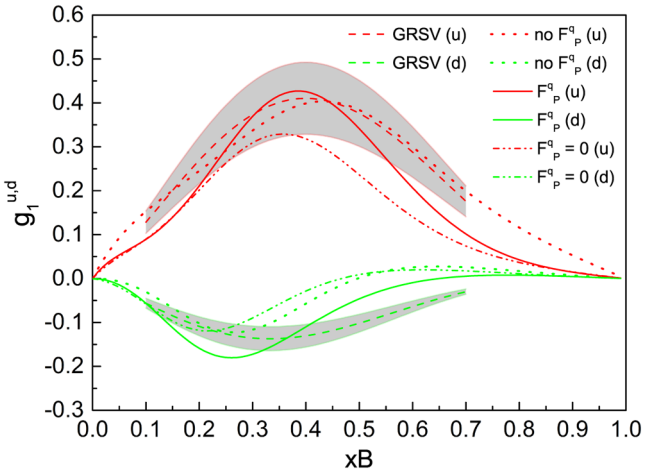

FIG. 3. The polarized PDF $g_1^{u,d}$ in our model. The red and blue lines are for u and d quark, respectively. The dashed lines are from GRSV2000 [48] and the shadow bands correspond to their relative error of 20.0%. Other curves are the same with the labels in Fig. 2.

$Q_0^2 = 0.26$ GeV^2 as a free parameter. In spite of the high χ^2 because we choose small relative errors for $f_1^{u,d}$, the agreement is acceptable for all the PDFs and the overall χ^2 is promoted significantly. The fit of f_1^u is as good as that in Fit-I, and the f_1^d is slightly improved. Though the description of g_1^u becomes a little worse in Fit-II, and the g_1^d is much better from $x = 0.3$ to 0.7. The contribution of the Pauli coupling is significant above $x = 0.3$, as can be seen in Figs. 2 and 3, when we turn it off in the fit results of Fit-II.

In Fig. 4, we give the predicted distributions $x\mathcal{C}^{u,d}(x)$ at $Q_0^2 = 0.26$ GeV^2 in our model. The magnitude of the u–quark distribution is much bigger than that of the d–quark, though their shapes are close to one another. The maximum for both distributions is around $x \simeq 0.4$.

TABLE I. Extracted parameters in two fit schemes. The † labels the parameter with a fixed value in the fit.

	Fit-I	Fit-II
m_q (GeV)	$0.3^\dagger$	$0.3^\dagger$
m_D^s (GeV)	0.769 ± 0.038	0.829 ± 0.025
$m_D^{a(u)}$ (GeV)	$1.5^\dagger$	$1.5^\dagger$
$m_D^{a(d)}$ (GeV)	0.857 ± 0.065	0.921 ± 0.007
Λ_s (GeV)	0.683 ± 0.028	0.545 ± 0.017
$\Lambda_{a(u)}$ (GeV)	0.767 ± 0.030	0.509 ± 0.025
$\Lambda_{a(d)}$ (GeV)	0.434 ± 0.027	0.385 ± 0.006
c_s^2	0.445 ± 0.048	0.657 ± 0.061
$c_{a(u)}^2$	1.245 ± 0.060	1.112 ± 0.089
$c_{a(d)}^2$	0.639 ± 0.011	0.662 ± 0.012
$\mathcal{F}_p^q(Q_0^2)$	$0.0^\dagger$	0.921 ± 0.117
χ^2/d.o.f	8.51	4.12

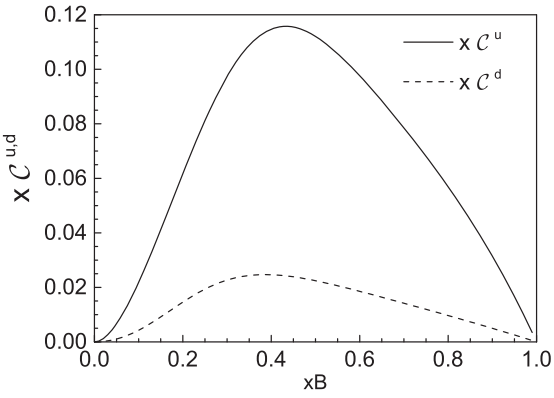

FIG. 4. The distributions $x\mathcal{C}^{u,d}(x)$ at $Q_0^2 = 0.26$ GeV^2 in our model. The solid and dashed lines are for u and d quark, respectively.

III. COMPARISON TO DATA OF cos 2ϕ_h ASYMMETRY

The $\cos 2\phi_h$ asymmetries in SIDIS off the hydrogen, deuterium, and ^{3}He targets have already been extensively explored by EMC [56], ZEUS [57,58], HERMES [59,60], COMPASS [61–64] Collaborations and at JLab [65–67]. Since both HERMES [59] and COMPASS [61] Collaborations have measured the SIDIS off the unpolarized proton for charged unidentified hadrons (h) among final particles but under slightly different Q^2, here we try to compare our new asymmetry in Eqs. (35) and (36) with the parameters in Table I to these data, together with the Cahn effect. We do not aim for a full analysis of the azimuthal asymmetry based on all released data because it is beyond the scope of this paper. Attempts in this direction can be found in a series of publications [5,11–16]. For the same reason, we also do not investigate the Boer-Mulders distribution [2] here, for which the Collins FFs of the production hadron should be introduced [3,4].

In the parton model, the SIDIS differential cross sections are expressed as the convolution of TMD PDFs $f_1(x, \boldsymbol{r}_\perp)$ and FFs $D_1^q(z_h, \boldsymbol{p}_\perp)$ [5,11–13],

$$\frac{d\sigma}{dxdydz_h dP_{hT}^2 d\phi_h} = \frac{2\pi\alpha^2}{Q^4 xy} \sum_q e_q^2 x \frac{y^2}{2(1-\varepsilon)} \left(1 + \frac{\gamma^2}{2x}\right) \times \int \mathrm{d}^2\boldsymbol{r}_\perp \mathrm{d}^2\boldsymbol{p}_\perp \delta^2(\vec{P}_{hT} - z_h\vec{r}_\perp - \vec{p}_\perp) \times f_1^q(x, \boldsymbol{r}_\perp) D_1^q(z_h, \boldsymbol{p}_\perp), \quad (40)$$

where the sum runs over the quark favor q. We denote by $\boldsymbol{P}_{hT}$ the transverse momentum of the final hadron h, and by $\boldsymbol{p}_\perp$ the transverse momentum of h with respect to the direction of the fragmenting quark. The $D_1^q(z_h, \boldsymbol{p}_\perp)$ is well recognized in the Gaussian form:

$$D_1^q(z_h,\boldsymbol{p}_\perp) = D_1^q(z_h)\frac{e^{-\boldsymbol{p}_\perp^2/\langle \boldsymbol{p}_\perp^2\rangle}}{\pi\langle \boldsymbol{p}_\perp^2\rangle}. \tag{41}$$

We adopt the unpolarized DSS FFs at leading order for $D_1^q(z_h)$ [68] with $\langle \boldsymbol{p}_\perp^2\rangle = 0.2$ GeV^2 [9,13]. The results do not change much if the SKMA FFs [69] are used instead.

Similarly, the contribution of the distribution $\mathcal{C}^q(x,\boldsymbol{r}_\perp)$ to the $\cos 2\phi_h$ asymmetry can be defined as

$$\begin{aligned}\frac{d\sigma}{dxdydz_h dP_{hT}^2 d\phi_h} &= \frac{2\pi\alpha^2}{Q^4 xy}\sum_q e_q^2 x\frac{y^2\varepsilon}{2(1-\varepsilon)}\left(1+\frac{\gamma^2}{2x}\right)\\ &\times\int d^2\boldsymbol{r}_\perp d^2\boldsymbol{p}_\perp \delta^2(\vec{P}_{hT}-z_h\vec{r}_\perp-\vec{p}_\perp)\\ &\times \mathcal{C}^q(x,\boldsymbol{r}_\perp)D_1^q(z_h,\boldsymbol{p}_\perp)\cos 2\phi_h. \end{aligned}\tag{42}$$

The Cahn effect on the $\cos 2\phi_h$ asymmetry can be obtained by substituting the $\mathcal{C}^q(x,\boldsymbol{r}_\perp)$ with the following function $\mathcal{C}^q_{cahn}(x,\boldsymbol{r}_\perp)$ in the above definition [70,71],

$$\mathcal{C}^q_{cahn}(x,\boldsymbol{r}_\perp) = 2\frac{2(\boldsymbol{r}_\perp\cdot\boldsymbol{h})^2-\boldsymbol{r}_\perp^2}{Q^2}f_1^q(x,\boldsymbol{r}_\perp), \tag{43}$$

with $\boldsymbol{h} = \boldsymbol{P}_{hT}/|\boldsymbol{P}_{hT}|$. As the only known one of the twist-4 effects, it is at the order of $\boldsymbol{r}_\perp^2/Q^2$, and hence it is controversial when we use the identical kinematical relations and factorization as the leading twist (see discussions in Refs. [12,13]). We have to leave these debates behind at present until these problems are completely resolved from the theoretical side.

The extracted value of $\mathcal{F}_P^q(Q_0^2)$ is close to 1.0 in Sec. II. This is, in fact, roughly compatible with the calculation in the instanton model [36], where it is found that the Q^2 dependence of the Pauli coupling can be parametrized very well by

$$\frac{\mathcal{F}_P^q(Q^2)}{\mathcal{F}_P^q(Q_0^2)} = \frac{1+\frac{\rho_c Q_0^2}{4.7m_q}}{1+\frac{\rho_c Q^2}{4.7m_q}}, \tag{44}$$

with the instanton size $\rho_c = 1/3$ fm. As a result, our new distribution is at the order of $1/Q^4$ and would suffer the same kinematical and dynamical problems as in the case of the Cahn effect as mentioned above. Moreover, the $\mathcal{F}_P^q$ decreases very rapidly below $Q^2 = 1.0$ GeV^2 and approaches a constant above 2.0 GeV^2. As a result, it is expected that the strength of the new asymmetry is enlarged in the very low Q^2. However, the data in this Q^2 range are unavailable. The average Q^2 of the HERMES [59] and COMPASS [61] measurements are about 2.5 and 3.0 GeV^2, respectively.[1] In principle, we need to evolve our distributions from Q_0^2 to the experimental one. Because the evolution of these distributions is not firmly established [17], we simply use the value of $\mathcal{F}_P^q(Q^2)$ at experimental Q^2, determined by Eq. (44) during our comparison. This leads to a reduction of about 1 order of magnitude of $\mathcal{C}^q(x,\boldsymbol{r}_\perp)$ compared to that at Q_0^2. It should be mentioned here that the data of EMC [56] and ZEUS [57,58] are measured in very high Q^2, so the contribution of both the Cahn effect and our new distribution to the $\cos 2\phi_h$ asymmetry are anticipated to be negligible.

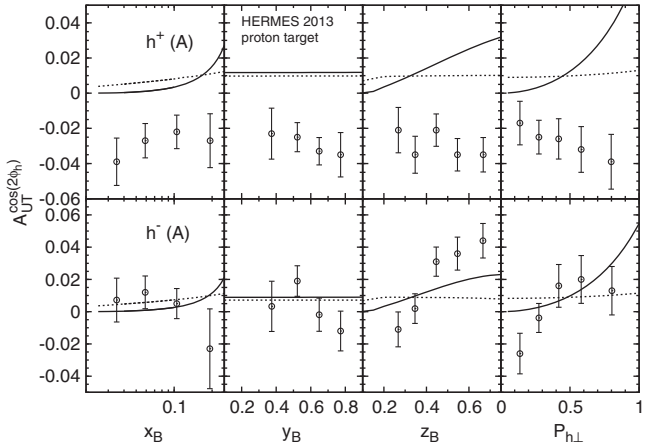

FIG. 5. The $A_{UT}^{\cos 2\phi_h}$ in one of kinematic ranges (A) of the HERMES measurement (see Table III in Ref. [59]). The solid and dotted curves are the results of Cahn effect and our new distribution, respectively.

The measured asymmetry in the experiment is defined as

$$A_{UT}^{\cos 2\phi_h} = \frac{\int d\sigma \cos 2\phi_h}{\int d\sigma}, \tag{45}$$

where the integrations are performed over the measured kinematical ranges of x, y, z_h, and P_{hT}, which can be found in the papers of the HERMES [59] and COMPASS [61] Collaborations. The detailed formalism of the integrations is found in Refs. [13,16].

Our calculated results are shown in Figs. 5 and 6, together with the corresponding data. As can be seen, the magnitude of the asymmetry induced by our new distribution is of a few percent and comparable to the Cahn effect in various kinematical ranges. The new and Cahn asymmetry are both flavor blind and positive for the $\pi^\pm$ inclusive production, while the Boer-Mulders effect is flavor dependent. Our asymmetry seems to be bigger than the Cahn effect in the kinematic range of the COMPASS measurement, as displayed in Fig. 6. Another feature is that our new asymmetry is more weakly dependent on the kinematical variables than the Cahn effect. In particular, it does not vanish when P_{hT} is approaching zero, as the Cahn effect does. The new asymmetry only begins to drop to zero when z is smaller than 0.2, as can be seen in Fig. 5. We arrive at the analogous conclusion for the identified charged

[1]There is strong correlation between variables x and Q^2 (and thus between x and y), but we put aside this problem at present and it should pay caution to the subfigures with the x variable in Figs. 5 and 6.

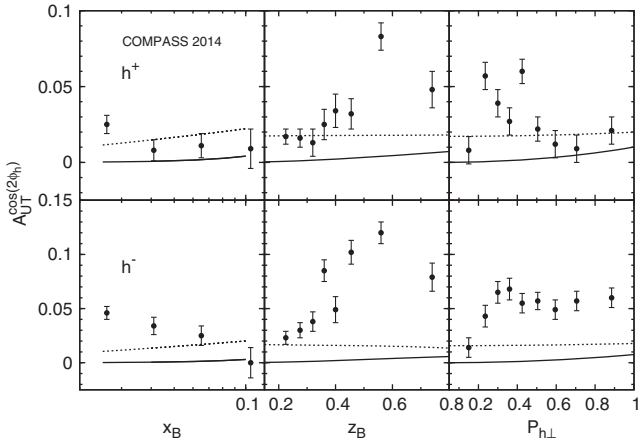

FIG. 6. The $A_{UT}^{\cos 2\phi_h}$ in kinematic range of the COMPASS measurement [61]. The solid and dotted curves are the results of Cahn effect and our new distribution, respectively.

pions and kaons produced by SIDIS off the nucleon, hydrogen, and deuterium targets.

It is concluded that the P_{hT} behavior of the COMPASS data seems to be incompatible with the corresponding behavior of HERMES data by Barone *et al.*[13]. Our new distribution in Eqs. (35) and (36) as functions of kinematical variables is unlike the Cahn effect, which is clearly illustrated in Figs. 5 and 6, so it would be helpful for understanding this inconsistency phenomenologically. A reliable extract of the Cahn and Boer-Mulders effects from experimental data should be done by considering the effect from our distribution $\mathcal{C}^q(x, \boldsymbol{r}_\perp)$.

IV. CONCLUSION

In summary, we investigate the role of the Pauli coupling in the photon-quark vertex to SIDIS. In the calculation, we utilize the scalar and axial-vector diquark models for the target nucleon. Our analytical formalism unveils that the obvious x dependence is introduced into the PDFs by this additional photon-quark vertex. We determine the Pauli coupling in the scale of $Q_0^2 = 0.26$ GeV^2 by fitting to the global fit of the PDFs. The determined value of the Pauli coupling agrees approximately with the prediction from the instanton model. The numerical results have shown that the Pauli coupling contributes considerably to the unpolarized and polarized PDFs in the low-Q^2.

Furthermore, we demonstrate that the Pauli coupling in the photon-quark vertex can cause the helicity flip of the struck quark, leading to a new positive $\cos 2\phi_h$ asymmetry in SIDIS. The magnitude of the asymmetry is proportional to the squared Pauli coupling, which introduces a significant Q^2 dependence into its evolution. If admitting this Q^2 dependence expediently from the instanton model, the given asymmetry is at the same level as the Cahn effect and of the order of a few percent in size within the HERMES and COMPASS kinematics. In other words, the magnitude of this new asymmetry is expected to be larger than that of the Cahn effect in the range of $Q^2 < 2.0$ GeV since it has a stronger Q^2 dependence than the Cahn effect. So the measurement of the Q^2 dependence of the $\cos 2\phi_h$ asymmetry is crucial to disentangle higher-twist effects and our new asymmetry.

The important observation is that the $\cos 2\phi_h$ asymmetry at the low Q^2 range should be explored systematically by including the effect from our distribution, together with the Cahn and Boer-Mulders effects. The available data of the $\cos 2\phi_h$ asymmetry in SIDIS do not yet allow a full extraction of the Boer-Mulders function due to the present kinematics which are still dominated by the low-Q^2 region. It is already found that the higher-twist contributions are of great significance and strongly affect the results of the fits [11,12]. The multidimensional data for the multiplicities released by HERMES [59] and COMPASS [61] Collaborations have large uncertainties, and they are also not sufficient for a full determination of the Boer-Mulders function [13]. Because the contribution of our new asymmetry is sizable, the experimental scrutiny of the Boer-Mulders function is more difficult. The future electron-ion colliders are anticipated to measure the $\cos 2\phi_h$ asymmetry in the higher Q^2 range where both our new asymmetry and other high-twist contribution, e.g., the Cahn effect, are expected to be small. We do not find any contribution of the Pauli coupling to the $\cos\phi_h$ azimuthal modulation, so the condition would be simpler there for the determination of the Boer-Mulders function.

It has been discovered that the Pauli couplings in both the photon-quark and photon-gluon vertices are contributing to the angular dependence of the SSA observables in polarized SIDIS [23,24]. Our calculations here complement earlier studies and accomplish a full picture of the influence of the helicity nonconservation interactions on the SIDIS measurements. The instantons are a possible underlying mechanism for these novel interactions, and they give the explicit Q^2 dependence of the corresponding couplings. Other optional approaches [72,73], e.g., Dyson-Schwinger equations with the nonperturbative quark and gluon propagators [74], are waiting to be extended to a nonzero photon virtuality before a feasible comparison of different models can be made.

ACKNOWLEDGMENTS

We gratefully acknowledge the enlightening discussions with Professor Vicente Vento, Professor Nikolai Kochelev, and Dr. Nikolai Korchagin at the initial stage of this work. We thank Dr. Ruilin Zhu and Dr. Wenjuan Mao for help in polishing the paper. We would like to thank Professor R. Sassot for sending us the files of DSS fragmentation functions and Dr. Rong Wang for the IMParton PDF files. This work was supported by the National Natural Science Foundation of China (Grant No. 11405222).

APPENDIX: $r_\perp$-INTEGRATED DISTRIBUTIONS

Her we list the $\boldsymbol{r}_\perp$-integrated results $f_1^{s,a}(x)$, $g_{1L}^{s,a}(x)$, and $\mathcal{C}^{s,a}(x)$ obtained in the context of our spectator diquark model:

$$f_1^s(x) = \frac{(1-x)^3}{(2\pi)^2}\frac{1}{24B_R^6(\Lambda_s^2)}\left[\left(\mathcal{F}_D^q - \frac{\mathcal{F}_P^q}{2m_q}D_Q\right)^2 B_R^2(\Lambda_s^2) + 2\left(\mathcal{F}_D^q + \frac{\mathcal{F}_P^q}{2m_q}D_R\right)^2 D_R^2 + \left(\frac{\mathcal{F}_P^q}{2m_q}\right)^2 B_R^2(\Lambda_s^2)(2B_R^2(\Lambda_s^2) + D_R^2)\right] \tag{A1}$$

$$\begin{aligned} f_1^a(x) = \frac{1-x}{(2\pi)^2}\frac{1}{24B_R^6(\Lambda_a^2)}\Bigg\{ & 2(1-x)^2\left[\left(\mathcal{F}_D^q + \frac{\mathcal{F}_P^q}{2m_q}D_R\right)D_R + \frac{\mathcal{F}_P^q}{2m_q}\frac{x}{1-x}B_R^2(\Lambda_s^2)\right]^2 \\ & + B_R^2(\Lambda_s^2)\Bigg[(\mathcal{F}_D^q + \mathcal{F}_P^q)^2x^2 + \left(\mathcal{F}_D^q + \frac{\mathcal{F}_P^q}{2m_q}(xD_R - D_Q)\right)^2 + \left(\frac{\mathcal{F}_P^q}{2m_q}\right)^2(2(1+2x^2)B_R^2(\Lambda_s^2) + (1-x)^2D_R^2) \\ & -2\left(\mathcal{F}_D^q + \frac{\mathcal{F}_P^q}{2m_q}D_R\right)\frac{\mathcal{F}_P^q}{2m_q}x(1-x)D_R\Bigg]\Bigg\} \end{aligned} \tag{A2}$$

$$g_{1L}^s(x) = \frac{(1-x)^3}{(2\pi)^2}\frac{1}{24B_R^6(\Lambda_s^2)}\left[-\left(\mathcal{F}_D^q - \frac{\mathcal{F}_P^q}{2m_q}D_Q\right)^2 B_R^2(\Lambda_s^2) + 2\left(\mathcal{F}_D^q + \frac{\mathcal{F}_P^q}{2m_q}D_R\right)^2 D_R^2 + \left(\frac{\mathcal{F}_P^q}{2m_q}\right)^2 B_R^2(\Lambda_s^2)(-2B_R^2(\Lambda_s^2) + D_R^2)\right] \tag{A3}$$

$$\begin{aligned} g_{1L}^a(x) = \frac{1-x}{(2\pi)^2}\frac{1}{24B_R^6(\Lambda_a^2)}\Bigg\{ & -2(1-x)^2\left[\left(\mathcal{F}_D^q + \frac{\mathcal{F}_P^q}{2m_q}D_R\right)D_R + \frac{\mathcal{F}_P^q}{2m_q}\frac{x}{1-x}B_R^2(\Lambda_s^2)\right]^2 \\ & + B_R^2(\Lambda_s^2)\Bigg[(\mathcal{F}_D^q + \mathcal{F}_P^q)^2x^2 + \left(\mathcal{F}_D^q + \frac{\mathcal{F}_P^q}{2m_q}(xD_R - D_Q)\right)^2 + \left(\frac{\mathcal{F}_P^q}{2m_q}\right)^2(2B_R^2(\Lambda_s^2) - (1-x)^2D_R^2) \\ & + 2\left(\mathcal{F}_D^q + \frac{\mathcal{F}_P^q}{2m_q}D_R\right)\frac{\mathcal{F}_P^q}{2m_q}x(1-x)D_R\Bigg]\Bigg\} \end{aligned} \tag{A4}$$

$$\mathcal{C}^s(x) = \frac{(1-x)^3}{(2\pi)^2}\frac{1}{24B_R^4(\Lambda_s^2)}\left(\frac{\mathcal{F}_P^q}{2m_q}\right)^2 2xMD_R \tag{A5}$$

$$\mathcal{C}^a(x) = \frac{(1-x)^2}{(2\pi)^2}\frac{1}{24B_R^4(\Lambda_a^2)}\left(\frac{\mathcal{F}_P^q}{2m_q}\right)^2\left[(1-x)D_R^2 + D_RD_Q + \frac{2B_R^2(\Lambda_s^2)}{1-x}x(1+x)\right] \tag{A6}$$

[1] V. Barone, F. Bradamante, and A. Martin, Prog. Part. Nucl. Phys. **65**, 267 (2010).
[2] D. Boer and P. J. Mulders, Phys. Rev. D **57**, 5780 (1998).
[3] J. C. Collins, Nucl. Phys. **B396**, 161 (1993).
[4] J. C. Collins, Phys. Lett. B **536**, 43 (2002).
[5] V. Barone, Z. Lu, and B. Q. Ma, Phys. Lett. B **632**, 277 (2006).
[6] A. Bacchetta, F. Conti, and M. Radici, Phys. Rev. D **78**, 074010 (2008).
[7] A. Bacchetta, A. Schaefer, and J. J. Yang, Phys. Lett. B **578**, 109 (2004).
[8] L. P. Gamberg, G. R. Goldstein, and M. Schlegel, Phys. Rev. D **77**, 094016 (2008).
[9] M. Anselmino, M. Boglione, U. D'Alesio, A. Kotzinian, F. Murgia, and A. Prokudin, Phys. Rev. D **71**, 074006 (2005).
[10] M. Anselmino, M. Boglione, J. O. Gonzalez Hernandez, S. Melis, and A. Prokudin, J. High Energy Phys. 04 (2014) 005.
[11] V. Barone, A. Prokudin, and B. Q. Ma, Phys. Rev. D **78**, 045022 (2008).
[12] V. Barone, S. Melis, and A. Prokudin, Phys. Rev. D **81**, 114026 (2010).
[13] V. Barone, M. Boglione, J. O. Gonzalez Hernandez, and S. Melis, Phys. Rev. D **91**, 074019 (2015).
[14] B. Zhang, Z. Lu, B. Q. Ma, and I. Schmidt, Phys. Rev. D **78**, 034035 (2008).
[15] Z. Lu and I. Schmidt, Phys. Rev. D **81**, 034023 (2010).
[16] B. Zhang, Z. Lu, B. Q. Ma, and I. Schmidt, Phys. Rev. D **77**, 054011 (2008).
[17] M. G. Echevarria, A. Idilbi, Z. B. Kang, and I. Vitev, Phys. Rev. D **89**, 074013 (2014).

[18] M. Boglione, S. Melis, and A. Prokudin, Phys. Rev. D **84**, 034033 (2011).
[19] B. Pasquini and P. Schweitzer, Phys. Rev. D **83**, 114044 (2011).
[20] P. Schweitzer, T. Teckentrup, and A. Metz, Phys. Rev. D **81**, 094019 (2010).
[21] Z. Wang, X. Wang, and Z. Lu, Phys. Rev. D **95**, 094004 (2017).
[22] N. Kochelev and N. Korchagin, Phys. Lett. B **729**, 117 (2014).
[23] P. Hoyer and M. Jarvinen, J. High Energy Phys. 10 (2005) 080.
[24] X. Cao, N. Korchagin, N. Kochelev, and P. Zhang, Phys. Rev. D **96**, 114010 (2017).
[25] D. Ostrovsky and E. Shuryak, Phys. Rev. D **71**, 014037 (2005).
[26] I. O. Cherednikov, U. D'Alesio, N. I. Kochelev, and F. Murgia, Phys. Lett. B **642**, 39 (2006).
[27] Y. Qian and I. Zahed, Ann. Phys. (Amsterdam) **374**, 314 (2016).
[28] T. Schäfer and E. V. Shuryak, Rev. Mod. Phys. **70**, 323 (1998).
[29] D. Diakonov, Prog. Part. Nucl. Phys. **51**, 173 (2003).
[30] N. I. Kochelev, Phys. Lett. B **426**, 149 (1998).
[31] N. Kochelev, H. J. Lee, B. Zhang, and P. Zhang, Phys. Lett. B **757**, 420 (2016).
[32] N. Kochelev, H. J. Lee, Y. Oh, B. Zhang, and P. Zhang, Phys. Rev. C **93**, 021901 (2016).
[33] N. Kochelev and N. Korchagin, Phys. Rev. D **89**, 034028 (2014).
[34] N. Kochelev, H. J. Lee, B. Zhang, and P. Zhang, Phys. Rev. D **92**, 034025 (2015).
[35] N. I. Kochelev, Phys. Lett. B **565**, 131 (2003).
[36] B. Zhang, A. Radzhabov, N. Kochelev, and P. Zhang, Phys. Rev. D **96**, 054030 (2017).
[37] R. Jakob, P. J. Mulders, and J. Rodrigues, Nucl. Phys. **A626**, 937 (1997).
[38] A. E. Dorokhov and I. O. Cherednikov, Phys. Rev. D **67**, 114017 (2003).
[39] X. d. Ji, J. p. Ma, and F. Yuan, Phys. Rev. D **71**, 034005 (2005).
[40] A. Bacchetta, M. Diehl, K. Goeke, A. Metz, P. J. Mulders, and M. Schlegel, J. High Energy Phys. 02 (2007) 093.
[41] E. Moffat, W. Melnitchouk, T. C. Rogers, and N. Sato, Phys. Rev. D **95**, 096008 (2017).
[42] A. Bacchetta, U. D'Alesio, M. Diehl, and C. A. Miller, Phys. Rev. D **70**, 117504 (2004).
[43] S. Dulat, T.-J. Hou, J. Gao, M. Guzzi, J. Huston, P. Nadolsky, J. Pumplin, C. Schmidt, D. Stump, and C.-P. Yuan, Phys. Rev. D **93**, 033006 (2016).
[44] L. A. Harland-Lang, A. D. Martin, P. Motylinski, and R. S. Thorne, Eur. Phys. J. C **75**, 204 (2015).
[45] R. D. Ball *et al.* (NNPDF Collaboration), J. High Energy Phys. 04 (2015) 040.
[46] S. Alekhin, J. Blumlein, and S. Moch, Phys. Rev. D **86**, 054009 (2012).
[47] M. Glück, E. Reya, and A. Vogt, Eur. Phys. J. C **5**, 461 (1998).
[48] M. Glück, E. Reya, M. Stratmann, and W. Vogelsang, Phys. Rev. D **63**, 094005 (2001).
[49] H. Abramowicz *et al.* (H1 and ZEUS Collaborations), Eur. Phys. J. C **75**, 580 (2015).
[50] X. Chen, J. Ruan, R. Wang, P. Zhang, and W. Zhu, Int. J. Mod. Phys. E **23**, 1450057 (2014).
[51] X. Chen, J. Ruan, R. Wang, P. Zhang, and W. Zhu, Int. J. Mod. Phys. E **23**, 1450058 (2014).
[52] D. de Florian, G. A. Navarro, and R. Sassot, Phys. Rev. D **71**, 094018 (2005).
[53] D. de Florian, R. Sassot, M. Stratmann, and W. Vogelsang, Phys. Rev. D **80**, 034030 (2009).
[54] M. Hirai, S. Kumano, and N. Saito (Asymmetry Analysis Collaboration), Phys. Rev. D **69**, 054021 (2004).
[55] F. Taghavi-Shahri, H. Khanpour, S. A. Tehrani, and Z. A. Yazdi, Phys. Rev. D **93**, 114024 (2016).
[56] M. Arneodo *et al.* (European Muon Collaboration), Z. Phys. C **34**, 277 (1987).
[57] J. Breitweg *et al.* (ZEUS Collaboration), Phys. Lett. B **481**, 199 (2000).
[58] S. Chekanov *et al.* (ZEUS Collaboration), Eur. Phys. J. C **51**, 289 (2007).
[59] A. Airapetian *et al.* (HERMES Collaboration), Phys. Rev. D **87**, 012010 (2013).
[60] F. Giordano and R. Lamb (HERMES Collaboration), J. Phys. Conf. Ser. **295**, 012092 (2011).
[61] C. Adolph *et al.* (COMPASS Collaboration), Nucl. Phys. **B886**, 1046 (2014).
[62] G. Sbrizzai (COMPASS Collaboration), J. Phys. Conf. Ser. **295**, 012043 (2011).
[63] W. Kafer (COMPASS Collaboration), arXiv:0808.0114.
[64] A. Bressan (COMPASS Collaboration), arXiv:0907.5511.
[65] X. Yan *et al.* (Jefferson Lab Hall A Collaboration), Phys. Rev. C **95**, 035209 (2017).
[66] M. Osipenko *et al.* (CLAS Collaboration), Phys. Rev. D **80**, 032004 (2009).
[67] H. Mkrtchyan *et al.*, Phys. Lett. B **665**, 20 (2008).
[68] D. de Florian, R. Sassot, and M. Stratmann, Phys. Rev. D **75**, 114010 (2007).
[69] M. Soleymaninia, A. N. Khorramian, S. M. Moosavi Nejad, and F. Arbabifar, Phys. Rev. D **88**, 054019 (2013).
[70] R. N. Cahn, Phys. Lett. **78B**, 269 (1978).
[71] R. N. Cahn, Phys. Rev. D **40**, 3107 (1989).
[72] Z. Lu and I. Schmidt, Phys. Rev. D **75**, 073008 (2007).
[73] A. Bacchetta and M. Radici, Phys. Rev. Lett. **107**, 212001 (2011).
[74] L. Chang, Y. X. Liu, and C. D. Roberts, Phys. Rev. Lett. **106**, 072001 (2011).